

Theoretical study of the structural and energetic properties of the ethane activation by single neutral and charged metal oxides

Federico Arrieta¹, Benjamín Figueredo², Marcos Rosa Brussin², Alan Hinchliffe³
and Humberto Soscún^{1*}

¹Laboratorio de Química Inorgánica, Departamento de Química, Facultad Experimental de Ciencias, La Universidad del Zulia, Apartado 526, Grano de Oro, Maracaibo, República Bolivariana de Venezuela. ²Escuela de Química, Universidad Central de Venezuela UCV, Caracas, República Bolivariana de Venezuela. ³School of Chemistry, The University of Manchester, Sackville Street, M60 1QD, UK.

Received: 30-09-05 Accepted: 15-11-05

Abstract

We present a theoretical study of the structural and energetic properties of the chemical activation of ethane (C_2H_6) in gas phase, by direct interaction with metal oxides such as $[MO]^0$, ($M = Ti, Cr, Fe, Ni, Zn$) and $[MO]^+$, ($M = V, Mn, Co, Cu, Ga$). The calculations were performed with the B3LYP method and the 6-31+G(d,p) basis set. The geometries were fully optimized and the results show that the M-O bonding energies of the charged species are lower than those of the neutral ones. For each series of the metal oxides, the bonding energies increase with the atomic number of M. The interaction between C_2H_6 and the MO, restricted to Cs symmetry, leads to the formation of different $[C_2H_6-MO]$ molecular complexes structures, which can be associated to the d electronic configuration of M. The structure of these complexes gives information about the preferences for the chemical activation of C_2H_6 by effect of the MO, that can be summarized as: a) $Ti(II)(d^2)$, $V(III)(d^2)$ and $Fe(II)(d^6)$, produce $[C_2H_6-M]$ adsorption complexes only; b) $Cr(II)(d^4)$, produce the alkyl and the hydride groups coordinated to the metal by σ bonds ($CH_3CH_2-Cr(O)-H$); c) $Mn(III)(d^4)$ and $Co(III)(d^6)$ activate the ethane towards the formation of ethanol adsorbed on the metal (CH_3CH_2OH-M); d) $Ni(II)(d^8)$ and $Cu(II)(d^9)$ activate ethane to the formation of alkyl and the hydroxyl groups coordinated by σ bonds to the metal (CH_3CH_2-M-OH), e) $Zn(II)(d^{10})$ and $Ga(III)(d^{10})$ give the formation of ethene and water adsorbed to the metal ($CH_2CH_2-M-H_2O$). The charged oxide species give higher reaction energies than the neutral ones.

Key words: *ab initio*; dehydrogenation; density functional theory methods; ethane; transition metal oxides.

* Autor para la correspondencia. Telf 0261-7598125, Cel. 04146113083.
E-mail: hsoscun@yahoo.es; hsoscun@hotmail.com

Estudio teórico de las propiedades estructurales y energéticas de la activación de etano mediante óxidos metálicos neutros y cargados

Resumen

El presente trabajo reporta una investigación teórica sobre las propiedades estructurales y energéticas de la activación química de etano (C_2H_6) en fase gaseosa, por interacción directa con una serie de óxidos neutros ($[MO]^0$, $M = Ti, Cr, Fe, Ni, Zn$) y cargados ($[MO]^+$, $M = V, Mn, Co, Cu, Ga$) de metales de transición y de no transición. Los cálculos fueron ejecutados utilizando el método B3LYP con el conjunto base 6-31+G(d,p). Las geometrías de los OM fueron optimizadas y los resultados indican que las energías de enlace de las especies cargadas son mucho menores que las de los óxidos neutros. Para cada serie MO, las energías de enlace se incrementan con el número atómico M. La interacción de C_2H_6 con los OM, restringida a simetría Cs, conduce a la formación de diferentes complejos moleculares $[C_2H_6-MO]$, las cuales se pueden asociar a la configuración electrónica d de M. Las estructuras de estos complejos permite observar las preferencias de la activación química del C_2H_6 por efecto del óxido metálico. Estos resultados pueden resumirse de la forma siguiente: a) $Ti(II)(d^2)$, $V(III)(d^2)$ y $Fe(II)(d^6)$, producen complejos de adsorción $[C_2H_6-M]$ solamente; b) $Cr(II)(d^4)$, produce que el grupo alquil y el ión hidruro estén coordinados al metal por enlaces tipo σ ($CH_3CH_2-Cr(O)-H$); c) $Mn(III)(d^4)$ y $Co(III)(d^6)$ activan el etano hacia la formación de etanol adsorbido sobre el metal (CH_3CH_2OH-M); d) $Ni(II)(d^8)$ y $Cu(III)(d^9)$ activan el etano hacia la formación de grupos alquilo y de grupos hidroxilo coordinados por enlaces tipo σ al metal (CH_3CH_2-M-OH), e) $Zn(II)(d^{10})$ and $Ga(III)(d^{10})$ conducen a la formación de eteno y agua adsorbidos al metal ($CH_2CH_2-M-H_2O$). Las especies cargadas dan valores de energías de reacción más altos que las especies neutras.

Palabras clave: *ab initio*; deshidrogenación; etano; óxidos de metales de transición; teoría del funcional densidad.

1. Introduction

The chemical conversion of light alkanes to important chemical products is an intense area of experimental (1 – 3) and theoretical research (4 – 6), where the permanent industrial necessity for light olefins requires new catalytic processes with the participation of new catalytic materials and not expensive operative conditions. Despite of major importance in the study of these catalytic processes, there is still a great controversy about the details of the involved mechanisms of reaction. One fundamental aspect in catalysis is the design and development of new catalytic materials and to achieve this goal a deep knowledge about the interaction

between reactants and catalytic surfaces is fundamental, which can be assessed by using either accurate experimental techniques or high level theoretical procedures.

Ethane is a light alkane that can suffer different catalytic reactions, such as dehydrogenation for the ethylene formation, oxidation to give ethanol and other more complicated reactions. For the case of ethane, it has been shown that a great variety of metal oxides, such as MgO , Al_2O_3 , SiO_2 , CaO , TiO_2 , V_2O_5 , Cr_2O_3 , Mn_3O_4 , Fe_3O_4 , ZnO , Ga_2O_3 , Y_2O_3 , ZrO_2 , Nb_2O_5 , MoO_3 , In_2O_3 , SnO_2 , La_2O_3 , CeO_2 , Ta_2O_5 and Tl_2O_3 , are able to catalyze the dehydrogenation of C_2H_6 (7 – 11). The dehydrogenation of light alkanes, such as

ethane, also can be occurs as a reaction of oxidative dehydrogenation over oxide catalysts using the oxygen molecule as oxidant compound. In fact, the direct conversion of ethane to ethylene is not commercially feasible due to the severe required conditions of high temperatures, side reactions, coke formation and catalyst deactivation. For the case of large alkanes, cracking also occur (12). For these class of reactions, the equilibrium conversion increases at higher temperatures. For this reason it is important the search of new catalytic systems that be able to reduce the operation temperatures that could help to minimize the side reactions.

Industrially, the Chromia/alumina is the catalytic system employed for the purpose of the dehydrogenation of alkanes with the formation of alkenes (13). However, there is no definitive conclusion on the origin of the catalytic activity of this complex catalyst system. In particular, the dehydrogenation activity of chromia catalyst is attributed to the Cr^{3+} which is an unsaturated coordinatively and is the most abundant species at low chromium contents. Also, the oxygen ions participate also in the reaction. In fact, the first step of the dehydrogenation process might involve the alkane adsorption with the participation of the oxygen ions bonded to the hydrogen atoms of the organic molecule (14), where the active site of the catalysts can be described as a Cr-O pair.

The present work is dedicated to the theoretical study of the direct ethane activation through single metal oxides M-O in gas phase.

2. Computational details

We have employed two kind of single metal oxides for the present study, the neutral $[\text{MO}]^0$, where the metal M corresponds to $\text{M} = \text{Ti}, \text{Cr}, \text{Fe}, \text{Ni}$ and Zn , and the charged ones $[\text{MO}]^+$, where the M corresponds to $\text{V}, \text{Mn}, \text{Co}, \text{Cu}$ and Ga . The geometries of these isolated metal oxides were optimized at the $C_{\infty v}$ symmetry. These oxides were forced to

perform direct interaction with ethane C_2H_6 until the formation of products, where both reactants started the interaction at the distance of 1.8 Å. The calculations were performed with the Gaussian 98 (15) computational package by using the Hartree-Fock HF and B3LYP (16) hybrid method of the density functional theory DFT. In particular, the optimizations of the MO oxides were carried out with the STO-3G (A), 3-21G** (B) and 6-31+G(d,p) (C) basis sets (17), whereas the optimized structure of the chemical interaction between the MO oxides and the ethane molecule was studied at the B3LYP/6-31+G(d,p) level of theory only. It is very important to note that these basis sets account for the total number of electrons in the metal oxide system.

To characterize the nature of the atomic interactions at the critical bonds of the metal oxides and those of the final products of the interaction between the metal oxides and ethane, calculations on the electronic density $\rho(r)$ of these systems were performed in the context of the theory of atoms in molecules of Bader et al (18) by using the AIM-PAC package (19). With this program we were able to evaluate at the HF/6-31+G(d) and B3LYP/6-31+G(d) levels of theory the topologic properties at the critical points of the $\rho(r)$, such as the electronic density $\rho(r_c)$ and the Laplacian of the density $\nabla^2 \rho(r_c)$. The electronic density $\rho(r_c)$ of the MO oxides and the interaction structures employed for the AIM-PAC calculations were constructed with the molecular orbitals calculated with the Gaussian software at the different levels of theory.

3. Results and Discussions

3.1. Structure, electronic population and energetic of the isolated metal oxides

The optimized M-O bond lengths in Angstroms (Å), the Mulliken atomic populations expressed as electronic charges of the

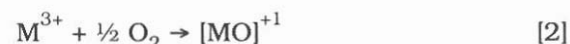
Metal $Q(M)$ and the oxygen $q(O)$ atoms, and the total energy of the $[MO]^0$ ($M = Ti, Cr, Fe, Ni$ and Zn) are displayed in Table I. The corresponding results for the $[MO]^{+1}$ ($M = V, Mn, Co, Cu$ and Ga) metal oxides, are reported in Table II. All these properties were calculated with the HF and the B3LYP methods and the STO-3G (A), 3-21G* (B) and 6-31+G(d) (C) basis sets.

The analysis of Table 1 results show that no systematic trends were found for the optimized M-O $[MO]^0$ bond lengths in terms of the nature of the basis sets. However, these effects are important for Cr, Fe, Ni and Zn metallic oxides and at HF/6-31+G(d,p) level it is observed that the M-O bond lengths increase drastically from TiO to ZnO, where the extension of the atomic basis function gives a larger spatial response to the increasing electrons in the metal oxide. The B3LYP method induces small changes in these optimized bond lengths. In this sense, we expect that the most reasonable geometry results are obtained with the B3LYP/6-31+G(d,p) approach. Similar analysis can be done for the results of the optimized bond distances of the $[MO]^{+1}$ metal oxides shown in Table 2. It is important to emphasize that for this system, the 3-21G* basis set give bond distances that are similar to those calculated with the extended 6-31+G(d,p) basis set. In this set of oxides, the MO bond distance decreases from VO to Mn, to increase to the CuO, and after decreases for the GaO. The behavior of the bond distances in terms of the atomic number can be observed in Figure 1 and Figure 2 for the $[MO]^0$ and $[MO]^{+1}$ oxides, respectively. The results show that the values of the optimized M-O bond lengths of both, the neutral and charged oxides, lies in the same scale of distance, which is from 1.5 Å to 1.75 Å.

The studied single oxides can be electronically characterized by their Mulliken atomic population and their energy, which are also displayed in Table 1 and Table 2 for the $[MO]^0$ and $[MO]^{+1}$ oxides, respectively. The effects of the basis sets are reflected in

these properties. However, for our analysis will be taken in account the B3LYP/6-31+G(d,p) property results. For the neutral oxides, the $Q(M)$ charges are almost constants and positive. For the charged ones, these charges are also positive and greater than 1.0, how is expected for the charge of the overall oxide. Additionally, the energy values are in order of the expectation for this kind of system and the different values are the response of the electronic species, were both systems lies in the same scale of energy.

For the studied oxides, it is important to account the oxygen bonding energy, which has been calculated by using the total energies of the species involved in the reactions:



The zero point energy correction was used for the evaluation of these M-O bonding energies. This property can be considered as an energetic index for accounting the strength of the oxygen atom in the oxide moiety, parameter that can be used to interpret the tendencies in the interaction of the oxides with different organic substrates. The corresponding HF/6-31+G(d,p) and B3LYP/6-31+G(d,p) results for the $[MO]^0$ and $[MO]^{+1}$ oxides are reported in Table 3. In Figures 3 and 4 are displayed the relationships between the bonding energy in Kcal/mol at B3LYP/6-31+G(d,p) level and the atomic numbers for the $[MO]^0$ and the $[MO]^{+1}$ metal oxides. Table 3 also reports the d^n configuration for each metal employed in the MO oxides, and the ratio between the bonding energy and the number of electrons (n) in the d orbital. This property, referred as the (E_b/n) ratio, is a measure of the energy by electron that is necessary to supply to the metal oxide to donate the oxygen atom in a chemical interaction. From these results, the GaO an ZnO^{+1} species are the metal oxides

Table 1
 Optimized geometric parameters (bond length in Å), Mulliken atomic population (electronic charges $Q(M)$ and $q(O)$ in e) and total energies (Hartrees) of the neutral metal oxides $[MO]^a$
 ($M = Ti, Cr, Fe, Ni$ and Zn).

Metal oxide	Method	Basis set	Bond length (M-O)	Charge $Q(M)$	Charge $q(O)$	Total Energy
TiO	HF B3LYP	A	1.590	0.287	-0.287	-913.5983
			1.611	0.181	-0.181	-914.8422
			1.421	0.438	-0.438	-1106.1152
CrO			1.449	0.314	-0.3142	-1107.5347
			1.400	0.403	-0.403	-1322.5211
FeO			1.413	0.251	-0.251	-1324.0549
			1.407	0.501	-0.501	-1563.8030
NiO			1.398	0.276	-0.276	-1565.4743
			1.387	0.590	-0.590	-1831.1859
ZnO			1.333	0.420	-0.420	-1832.8647
			1.571	0.516	-0.516	-918.6827
			1.591	0.314	-0.314	-920.1343
CrO			1.541	0.589	-0.589	-1112.4984
			1.538	0.356	-0.356	-1114.1364
FeO			1.557	0.435	-0.435	-1332.2771
			1.681	0.568	-0.568	-1573.7425
NiO			1.565	0.491	-0.491	-1575.6566
			1.675	0.593	-0.593	-1843.4661
ZnO			1.609	0.472	-0.472	-1845.4722
			1.554	0.716	-0.716	-923.1342
			1.594	0.523	-0.557	-924.5926
CrO			1.574	0.759	-0.759	-1117.8585
			1.555	0.535	-0.535	-1119.5078
FeO			1.618	0.842	-0.842	-1336.8612
			1.551	0.554	-0.554	-1338.6938
NiO			1.628	0.758	-0.758	-1581.2784
			1.625	0.531	-0.531	-1583.2814
ZnO			1.738	0.664	-0.664	-1852.2521
			1.712	0.614	-0.614	-1854.2966

Table 2
 Optimized geometric parameters (bond length in Å), Mulliken atomic population (electronic charges $Q(M)$ and $q(O)$ in e) and total energies (Hartrees) of the charged metal oxides $[MO]^{\pm 1}$
 (M = V, Mn, Co, Cu and Ga).

Metal oxide	Method	Basis set	Bond length (M-O)	Charge $Q(M)$	Charge $q(O)$	Total Energy
VO	HF B3LYP	A	1.463	1.071	-0.071	-1006.6971
			1.503	0.977	+0.023	-1008.0296
MnO			1.441	1.398	-0.398	-1210.9635
			1.412	1.077	-0.077	-1212.5462
CoO			1.514	1.249	-0.249	-1439.7049
			1.408	1.172	-0.172	-1441.2817
CuO			1.440	1.284	-0.284	-1693.8109
			1.393	1.203	-0.203	-1695.4531
GaO			1.358	1.312	-0.312	-1974.4681
			1.376	1.210	-0.210	-1976.1542
VO	HF B3LYP	B	1.522	1.508	-0.508	-1012.4418
			1.543	1.323	-0.323	-1013.9290
MnO			1.536	1.513	-0.513	-1218.0890
			1.539	1.204	-0.204	-1219.8054
CoO			1.640	1.220	-0.220	-1448.5380
			1.578	1.370	-0.370	-1450.3706
CuO			1.625	1.224	-0.224	-1704.8980
			1.589	1.206	-0.206	-1706.8785
GaO			1.868	1.134	-0.134	-1988.0507
			1.715	1.156	-0.156	-1990.0359
VO	HF B3LYP	C	1.504	1.375	-0.375	-1017.3287
			1.531	1.152	-0.152	-1018.8346
MnO			1.439	1.257	-0.257	-1223.9594
			1.469	1.047	-0.047	-1225.6843
CoO			1.525	1.244	-0.244	-1455.4812
			1.562	1.088	-0.088	-1457.3930
CuO			2.249	0.866	+0.134	-1713.1292
			1.728	0.981	+0.019	-1715.0640
GaO			1.833	1.089	-0.089	-1995.6593
			1.702	1.107	-0.107	-1997.7096

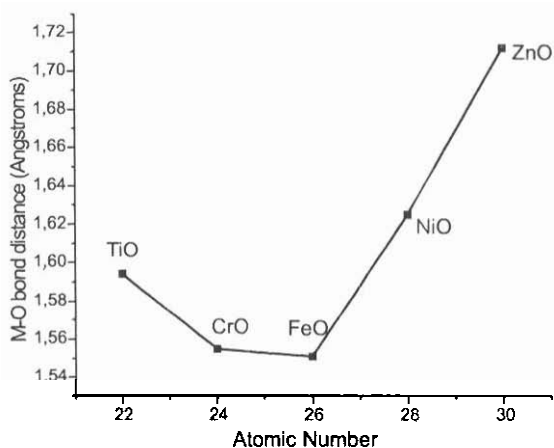


Figure 1. Relationship between the M-O (B3LYP/6-31+G(d,p)) bond distances and the atomic numbers of the $[MO]^0$ (M = Ti, Cr, Fe, Ni, Zn) metal oxides.

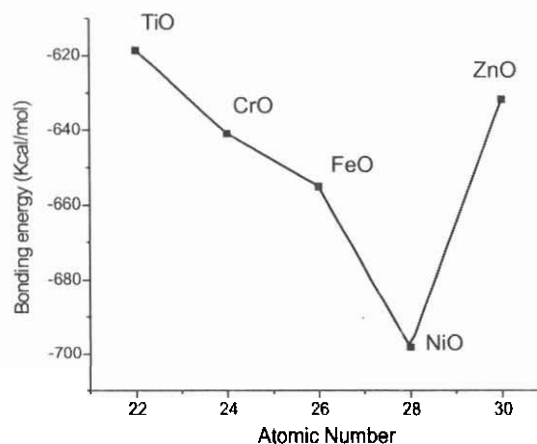


Figure 3. Relationship between the bonding energy in Kcal/mol at B3LYP/6-31+G(d,p) level and the atomic numbers of the $[MO]^0$ (M = Ti, Cr, Fe, Ni, Zn) metal oxides

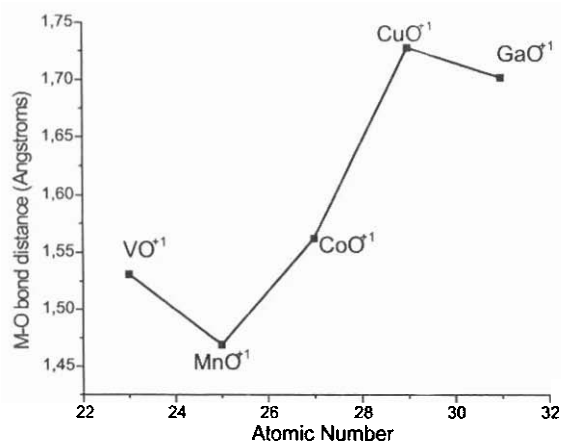


Figure 2. Relationship between the M-O (B3LYP/6-31+G(d,p)) bond distances and the atomic numbers of the $[MO]^1$ (M = V, Mn, Co, Cu, Ga) metal oxides.

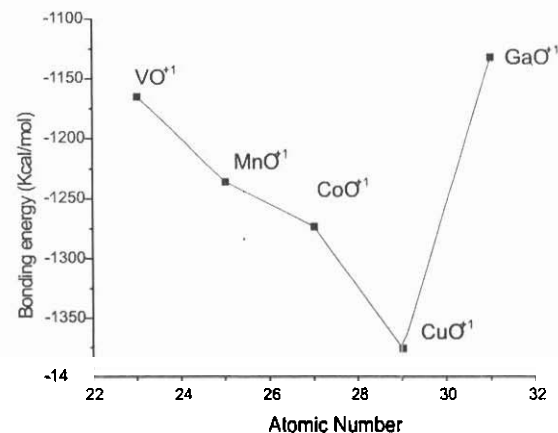


Figure 4. Relationship between the bonding energy in Kcal/mol at B3LYP/6-31+G(d,p) level and the atomic numbers of the $[MO]^1$ (M = V, Mn, Co, Cu, Ga) metal oxides.

des that are able to donate the O atom easier than the rest of studied compounds.

3.2. Topologic analysis of the electronic density XX of the isolated metal oxides

The charge density of the series of the isolated $[MO]^0$ and the $[MO]^1$ metal oxides has been studied by using the atoms in mole-

cules AIM theory through the analysis of the topology of the electronic density $\rho(r)$. In this sense, the critical point of the M-O bond BCP has been characterized by the evaluation at the position of the critical point of both, the charge density $\rho(r_c)$ and the Laplacian of the

Table 3
M-O Bonding energy (Kcal/mol) of the metal oxides [MO], calculated at the HF/6-31+G(d,p) and B3LYP/6-31+G(d,p) levels of theory

[MO] ⁰	Bonding energy (Kcal/mol)		[MO] ⁺¹	Bonding energy (Kcal/mol)	
	HF/ 6-31+G(d,p)	B3LYP/ 6-31+G(d,p)		HF/ 6-31+G(d,p)	B3LYP/ 6-31+G(d,p)
[TiO] ⁰ (d ²)	-501.0	-618.5 (-309,3)	[VO] ⁺¹ (d ²)	-1020.7	-1165.1 (-582,5)
[CrO] ⁰ (d ⁴)	-492.8	-640.9 (-160,2)	[MnO] ⁺¹ (d ⁴)	-1046.2	-1235.8 (-308,9)
[FeO] ⁰ (d ⁶)	-491.5	-655.1 (-109,2)	[CoO] ⁺¹ (d ⁶)	-1055.6	-1273.2 (-212,2)
[NiO] ⁰ (d ⁸)	-532.5	-698.1 (-87,3)	[CuO] ⁺¹ (d ⁸)	-1243.4	-1375.5 (-171,9)
[ZnO] ⁰ (d ¹⁰)	-530.5	-631.7 (-63,2)	[GaO] ⁺¹ (d ¹⁰)	-1031.4	-1132.1 (-113,2)

charge density $\nabla^2 \rho(r_c)$. The $\rho(r_c)$ is a property that is a measure of the degree of the charge concentration of the bond and is an indication of the order of such bond. The $\nabla^2 \rho(r_c)$ is a property that reflect if the bond at the critical point is dominated by either ionic or covalent interactions. These properties were calculated at the HF and B3LYP with the 6-31+G(d,p) basis set and the corresponding results are reported in Table 4. These results show that for the studied oxides, [MO]⁰ and [MO]⁺¹ compounds, the density of charge $\rho(r_c)$ decreases from the oxides with low number of d electrons to those oxides were the metal has high number of d electrons. In particular, those elements such as Zn and Ga give single oxides were the charge density at the critical point of the M-O bond is lower than their corresponding homologue oxides. These results indicate that the ZnO and GaO⁺¹ have the lower bond order in both series of metal oxides.

On the other hand, the Laplacian $\nabla^2 \rho(r_c)$ of the studied oxides have positive values for all the studied oxides indicating,

that these M-O bonds are dominated by ionic interactions how was expected. No systematic variations was found for the $\rho(r_c)$ and the $\nabla^2 \rho(r_c)$ with the previous studied properties of the oxides. However, a linear correlation with high correlation coefficient was found between the binding energy by electron and the $\rho(r_c)$ at HF/6-31+G(d,p) for the [MO]⁰ series. A similar relations hip with lower correlation coefficient was found for the cationic metal oxides. These results indicate that in some complicated way the binding energy by electron and the degree of charge concentration are related in the metal oxides.

It is important to mention that the associated properties to $\rho(r_c)$ are affected by the electron correlation how can be seen from results reported in Table 4.

3.3. Interaction between the single metal oxides and ethane

In this section are presented the results of the direct interaction between the metal oxides and the ethane (C₂H₆) molecule, that were determined by the geometry op-

Table 4
Topologic properties at the critical points of the metal oxides [MO] (total density $\rho(r_c)$ and Laplacian of the charge density $\nabla^2\rho(r_c)$) calculated at the HF/6-31+G(d,p) and B3LYP/6-31+G(d,p) levels of theory.

[MO]] ^o	$\rho(r_c)$		$\nabla^2\rho(r_c)$	
	HF	B3LYP	HF	B3LYP
TiO	0.337	0.295	0.64	0.81
CrO	0.292	0.300	1.08	1.23
FeO	0.231	0.277	1.43	1.61
NiO	0.209	0.211	1.35	1.33
ZnO	0.144	0.154	0.52	0.52
[MO]] ⁺¹	HF	B3LYP	HF	B3LYP
VO	0.362	0.332	1.64	0.83
MnO	0.414	0.365	0.67	1.10
CoO	0.284	0.258	2.43	2.01
CuO	0.042	0.159	0.21	1.00
GaO	0.094	0.139	0.36	0.77

timization at the B3LYP/6-31+G(d,p) level of theory and the corresponding optimized geometric parameters (bond lengths in Angstroms, bond angles and bond dihedral angles in degrees) are reported in Table 5. The labels of these parameters correspond to those shown in scheme I for the neutral oxides and in scheme II for the cationic ones, were the optimized structures of the final products of the M-O — C₂H₆ interaction are displayed.

The detailed analysis of the optimized parameters of the final structures of the M-O — C₂H₆ interaction is not worth since the geometric point of view. However it is important to analyze the kind of final product of these interactions. In fact, these pictures show the way how the ethane molecule can be activated by a direct chemical (or physical) interaction of a wide variety of single transition metal oxides, including Zn and Ga. A simple inspection to these structures shows that there is a close analogy in the kind of interaction with respect

to the d configuration of the metal involved either in the neutral or cationic oxides. For example, Ti(II) and V(III) belong to the d² configuration and these metals are able to form similar adsorbed complexes between the oxide and ethane. For the cases of Cr(II) and Mn(III) that belong to the d⁴ configuration, there is not similarity between the products, were the CrO-C₂H₆ interaction activates the C-H bond with formation of the CH₃CH₂ alkyl group in a complex of the type H-CrO-CH₂CH₃. Instead, the MnO-C₂H₆ interaction activates the organic substrate with the formation of ion Mn adsorbed in the structure of ethanol (Mn-C₂H₅OH).

The Fe(II) and Co(III) have d⁶ configuration and their behaviors are also different. For example, the FeO is able to adsorb the ethane only without any chemical perturbation, while the CoO⁺¹ oxide activate the ethane with the subsequent formation of ion Co adsorbed on ethanol (Co-C₂H₅OH). This interaction is similar to that of MnO⁺¹.

Table 5

Bond lengths (Å) and bond angles (°) of the optimized final products of the interaction between the metal oxides $[M-O]^{0/+1}$ and ethane, calculated at the B3LYP/6-31+G(d,p). The labels of the geometric parameters correspond to those from scheme I for $[M-O]^0$ and scheme II for $[M-O]^{+1}$.

	TiO	VO ⁺¹	CrO	MnO ⁺¹	FeO	CoO ⁺¹	NiO	CuO ⁺¹	ZnO	GaO ⁺¹
Bond lengths/Å										
R(1-2)	1.649	1.547	1.546	1.996	1.602	1.881	1.740	1.722	1.790	2.144
R(1-3)	2.908	2.631	3.123	2.618	3.989	2.626	2.135	2.193	3.297	4.562
R(1-4)	2.811	2.517	1.978	2.838	3.102	2.786	1.855	1.928	3.481	5.022
R(1-9)	2.274	2.130	3.145	1.844	6.696	1.817	1.701	1.791	1.516	2.873
R(2-4)	3.493	3.438	3.155	1.455	4.704	1.466	3.063	2.980	3.767	3.156
R(2-3)	4.182	4.033	3.779	2.416	5.520	2.408	3.819	3.794	4.194	3.157
R(2-10)	2.425	2.430	2.670	0.968	3.597	0.989	0.963	0.969	0.964	0.972
R(3-4)	1.549	1.559	1.539	1.543	1.541	1.537	1.502	1.495	1.336	1.342
R(3-5)	1.094	1.092	1.095	1.092	1.093	1.091	1.092	1.094	1.0870	1.088
R(3-6)	1.094	1.092	1.095	1.092	1.093	1.091	1.092	1.094	1.0870	1.088
R(3-9)	1.106	1.115	1.095	1.128	1.093	1.128	1.160	1.154	3.441	2.184
R(4-7)	1.094	1.092	1.109	1.093	1.092	1.092	1.090	1.089	1.087	1.088
R(4-8)	1.094	1.092	1.109	1.093	1.092	1.092	1.090	1.089	1.087	1.088
R(4-10)	1.105	1.121	3.081	2.049	1.111	2.073	3.221	3.118	3.237	3.361
Bond angles/°										
A(1,3,4)	70.9	68.4	31.4	81.6	45.2	79.3	58.3	59.5	86.5	102.3
A(2,1,3)	131.2	148.6	102.8	61.4	159.8	62.0	160.3	151.3	107.3	37.9
A(2,4,3)	105.5	100.8	101.6	107.3	114.3	106.6	108.7	111.6	99.2	77.8
A(5,3,6)	107.4	108.3	107.2	108.5	107.7	109.4	110.9	113.3	116.4	117.0
A(7,4,8)	107.3	108.6	105.0	109.5	108.3	110.1	112.8	115.7	116.6	116.8
A(9,3,5)	104.8	103.1	107.0	102.8	107.3	104.0	101.9	101.1	78.8	100.8
A(9,3,6)	104.8	103.1	107.0	102.8	107.3	104.0	101.9	101.1	78.8	100.8
A(10,4,7)	105.3	102.2	83.7	94.6	105.7	94.4	89.6	81.5	78.9	89.4
A(10,4,8)	105.3	102.2	83.7	94.6	105.7	94.4	89.6	81.5	78.9	89.4
Dihedral angles/°										
D(1,2,4,3)	0.0	0.0	180.0	0.0	0.0	0.0	0.0	0.0	0.0	0.0
D(1,3,4,7)	-120.8	-120.0	-121.2	-118.8	-118.2	-117.9	-111.0	-104.1	-90.5	-92.0
D(1,3,4,8)	120.8	120.0	121.2	118.8	118.2	117.9	111.0	104.1	90.5	92.0
D(1,3,4,10)	0.0	0.0	0.0	0.0	0.0	0.0	0.0	0.0	0.0	0.0
D(2,4,3,5)	120.0	120.0	120.1	119.2	120.0	118.7	114.8	114.8	90.5	92.3
D(2,4,3,6)	-120.0	-120.0	-120.1	-119.2	-120.0	-118.7	-114.8	-114.8	-90.5	-92.3
D(2,4,3,9)	0.0	0.0	0.0	0.0	0.0	0.0	0.0	0.0	0.0	0.0

On the other hand, the Ni and Cu with formal (II) and III charges, respectively, have d^8 configuration. The corresponding oxides of these metals interact with ethane in the same way giving the formation of the OH group bonded to the metal and the formation of the CH_3CH_2 alkyl group. Here it is worth to mention that the coordination of this alkyl group to the metal occurs through a σ bond.

For the cases of Zn and Ga that belong to the d^{10} configuration, the corresponding oxides activate the ethane compound to the dehydrogenation a reaction with the formation of ethane. In particular, the ZnO activates ethane to ethene with the formation of the OH group bonded to the Zn-H species. However, the GaO^+ activates the ethane with the formation of ethene and water adsorbed on the Ga ion.

The energetic of the final products can be expressed from the values of the interaction energies, which values are reported in Table 6. This property has been evaluated at by using the equation

$$\text{Interaction energy} = E_T(\text{final productos}) - E_T(\text{metal oxide}) - E_T(\text{ethane}) \quad [3]$$

where the E_T corresponds to the B3LYP/6-31+G(d,p) total energy of the species. The results of Table 6 indicate that the interaction energies are lower for the neutral oxides than for the charged ones. For the

neutral oxides, no systematic variation was observed between the interaction energies and previous studied properties. However, for the charged ones, the energy of interaction increases with the atomic number of the metal.

3.4. Topologic analysis of the electronic density $\rho(r)$ of the interaction between the metal oxides and ethane

From Table 7 to Table 12 are reported the results of the topology of the charge density ($\rho(r_c)$ and $\nabla^2 \rho(r_c)$) calculated at the position of the critical point of the bond paths of the structures of the final products of scheme I and II. These results show the electronic features of the dominant atomic interactions in the final products of the activation of ethane from metal oxides.

The analyses the results of Table 7 show that for the TiO and VO^+ metal oxide complexes, the values of the $\rho(r_c)$ and $\nabla^2 \rho(r_c)$ at the BCP of the M-O bond path are not strongly affected by the ethane interaction. This is expected due to the nature of the final product that corresponds to the ethane molecule adsorbed on the metal oxide. For the CrO-ethane (Table 8), the properties of the M-O bond remain almost constant after the interaction. Due to the strong interaction between the MnO and CoO cationic species with ethane, where the M-O bond is broken with the formation of ethanol, the co-

Table 6
Interaction energy E_i (kcal/mol) of the ethane molecule with the metal oxides, calculated at the B3LYP/6-31+G(d,p) level of theory.

$[\text{MO}]^0$	Interaction energy E_i (Kcal/mol)	$[\text{MO}]^{+1}$	Interaction energy E_i (Kcal/mol)
$[\text{TiO}]^0$	-5.96	$[\text{VO}]^{+1}$	-22.86
$[\text{CrO}]^0$	-25.83	$[\text{MnO}]^{+1}$	-69.37
$[\text{FeO}]^0$	6.73	$[\text{CoO}]^{+1}$	-89.77
$[\text{NiO}]^0$	-70.67	$[\text{CuO}]^{+1}$	-117.16
$[\text{ZnO}]^0$	-52.87	$[\text{GaO}]^{+1}$	-131.59

Table 7

Topologic properties at the critical points of the complexes between $[\text{TiO}]^0$ and $[\text{VO}]^{+1}$ and ethane (total density $\rho(r_c)$ and Laplacian of the charge density $\nabla^2 \rho(r_c)$) calculated at the B3LYP/6-31+G(d,p) level of theory. See scheme I and II for labels.

Bond path	Total density		Laplacian of the charge density	
	$[\text{TiO}]^0$	$[\text{VO}]^{+1}$	$[\text{TiO}]^0$	$[\text{VO}]^{+1}$
r(1-2)	0.241	0.316	+0.75	+0.87
r(1-9)	0.183	0.300	+0.71	+0.10
r(1-10)	0.021	0.039	+0.15	+0.23
r(3-4)	0.232	0.226	-0.51	-0.48
r(3-5)	0.279	0.283	-0.97	-1.03
r(3-6)	0.279	0.283	-0.97	-1.03
r(3-9)	0.262	0.253	-0.82	-0.75
r(4-7)	0.279	0.284	-0.97	-1.03
r(4-8)	0.279	0.284	-0.97	-1.03
r(4-10)	0.268	0.250	-0.88	-0.73

Table 8

Topologic properties at the critical points of the complex between $[\text{CrO}]^0$ and ethane (total density $\rho(r_c)$ and Laplacian of the charge density $\nabla^2 \rho(r_c)$) calculated at the B3LYP/6-31+G(d,p) level of theory. See scheme I and II for labels.

Bond path	Total density $\rho(r_c)$	Laplacian of the charge density $\nabla^2 \rho(r_c)$
r(1-2)	0.306	+0.94
r(1-4)	0.127	+0.16
r(1-10)	0.112	+0.14
r(3-4)	0.234	-0.51
r(3-5)	0.276	-0.94
r(3-6)	0.276	-0.94
r(3-9)	0.277	-0.95
r(4-7)	0.261	-0.81
r(4-8)	0.261	-0.81

Corresponding results of the $\rho(r_c)$ and $\nabla^2 \rho(r_c)$ properties at the BCP of the M-O bond path change strongly by effects of the interaction. These results can be seen in Table 9. The topology results for FeO-ethane interaction are shown in Table 10. For the cases of NiO

and CuO^{+1} interactions with ethane, the results of topology for the specific M-O bond path varies slowly, mainly for the case of NiO, which results are reported in Table 11. It is important to note at this point that the corresponding results of the topology for the

Table 9

Topologic properties at the critical points of the complex between $[\text{MnO}]^{+1}$ and $[\text{CoO}]^{+1}$ and ethane (total density $\rho(r_c)$ and Laplacian of the charge density $\nabla^2\rho(r_c)$) calculated at the B3LYP/6-31+G(d,p) level of theory. See scheme I and II for labels.

Bond path	Total density		Laplacian of the charge density $\nabla^2\rho(r_c)$	
	$[\text{MnO}]^{+1}$	$[\text{CoO}]^{+1}$	$[\text{MnO}]^{+1}$	$[\text{CoO}]^{+1}$
r(1-2)	0.806	0.086	+0.45	+0.65
r(1-9)	0.034	0.049	+0.30	+0.13
r(2-4)	0.225	0.218	-0.27	-0.25
r(2-10)	0.355	0.353	-2.14	-2.14
r(3-4)	0.243	0.246	-0.57	-0.58
r(3-5)	0.283	0.283	-1.02	-1.03
r(3-6)	0.283	0.283	-1.02	-1.03
r(3-9)	0.243	0.242	-0.68	-0.68
r(4-7)	0.292	0.292	-1.10	-1.10
r(4-8)	0.292	0.292	-1.10	-1.10

Table 10

Topologic properties at the critical points of the complex between FeO and ethane (total density $\rho(r_c)$ and Laplacian of the charge density $\nabla^2\rho(r_c)$) calculated at the B3LYP/6-31+G(d,p) level of theory. See scheme I and II for labels.

Bond path	Total density* $\rho(r_c)$	Laplacian of the charge density $\nabla^2\rho(r_c)$
r(1-2)	0.242	+1.18
r(1-10)	0.029	+0.08
r(3-4)	0.238	-0.54
r(3-5)	0.281	-0.99
r(3-6)	0.281	-0.99
r(3-9)	0.252	-0.74
r(4-7)	0.278	-0.96
r(4-8)	0.278	-0.96
r(4-10)	0.278	-0.96

C-C and C-H bonds of the ethane moiety are similar to those of the isolated ethane. The topology results for the complex of activation of ethane with ZnO and GaO^{+1} are

shown in Table 12, where important changes are observed for the properties of the bond path of these oxides. Significant effects are observed in the topology of the GaO^{+1}

Table 11

Topologic properties at the critical points of the complexes between $[\text{NiO}]^0$ and $[\text{CuO}]^{+1}$ and ethane (total density $\rho(r_c)$ and Laplacian of the charge density) calculated at the B3LYP/6-31+G(d,p) level of theory. See scheme I and II for labels.

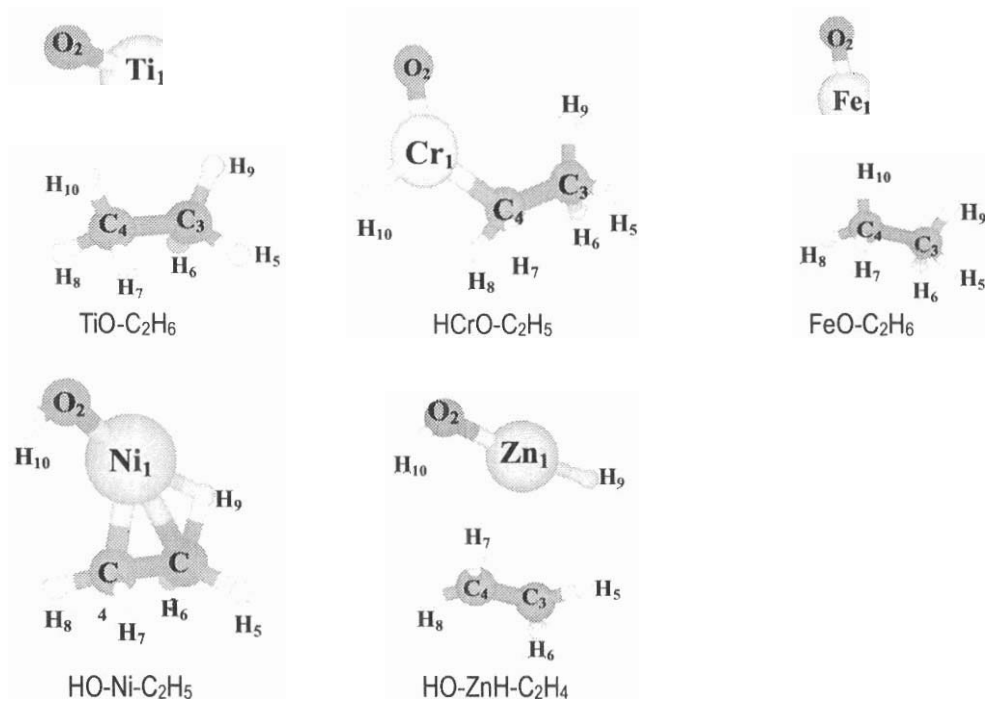
Bond path	Total density $\rho(r_c)$		Laplacian of the charge density $\nabla^2\rho(r_c)$	
	$[\text{NiO}]^0$	$[\text{CuO}]^{+1}$	$[\text{NiO}]^0$	$[\text{CuO}]^{+1}$
r(1-2)	0.152	0.160	+0.86	+0.79
r(1-3)	0.071	0.065	+0.27	+0.21
r(1-4)	0.141	0.112	+0.18	+0.01
r(1-9)	0.071	0.066	+0.28	+0.18
r(2-10)	0.362	0.353	-2.01	-2.65
r(3-4)	0.254	0.260	-0.57	-0.62
r(3-5)	0.280	0.282	-0.99	-1.04
r(3-6)	0.280	0.282	-0.99	-1.04
r(3-9)	0.229	0.228	-0.59	-0.59
r(4-7)	0.280	0.289	-0.98	-1.12
r(4-8)	0.280	0.289	-0.98	-1.12

Table 12

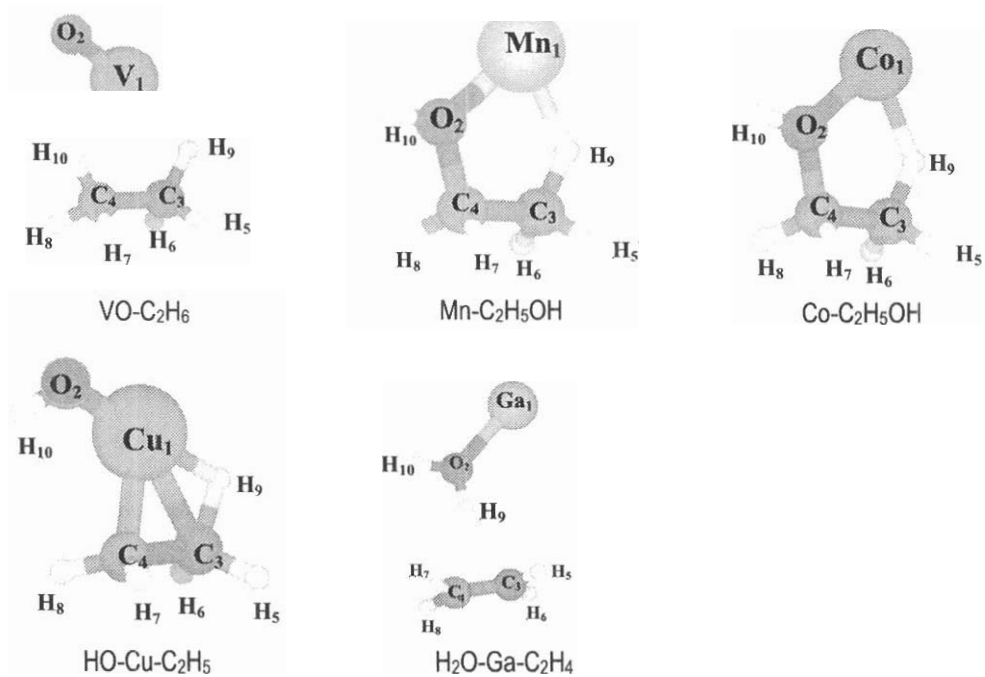
Topologic properties at the critical points of the complexes between $[\text{ZnO}]^0$ and $[\text{GaO}]^{+1}$ and ethane (total density $\rho(r_c)$ and Laplacian of the charge density $\nabla^2\rho(r_c)$) calculated at the B3LYP/6-31+G(d,p) level of theory. See scheme I and II for labels.

Bond path	Total density $\rho(r_c)$		Laplacian of the charge density $\nabla^2\rho(r_c)$	
	$[\text{ZnO}]^0$	$[\text{GaO}]^{+1}$	$[\text{ZnO}]^0$	$[\text{GaO}]^{+1}$
r(1-2)	0.134	0.552	0.62	+0.20
r(1-3)	0.008	-	0.02	-
r(1-9)	0.126	-	0.03	-
r(2-9)	-	0.317	-	-1.81
r(2-10)	0.361	0.349	-1.99	-2.07
r(3-4)	0.345	0.342	-1.01	-1.00
r(3-5)	0.284	0.284	-1.03	-1.04
r(3-6)	0.284	0.284	-1.03	-1.04
r(4-7)	0.283	0.285	-1.02	-1.04
r(4-8)	0.283	0.285	-1.02	-1.04

Scheme I



Scheme II



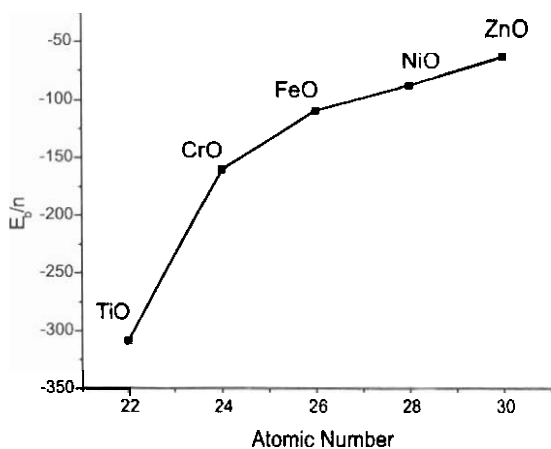


Figure 5. Relationship between the E_b/n ratio at B3LYP/6-31+G(d,p) and the atomic number of the $[MO]^0$ ($M = \text{Ti, Cr, Fe, Ni, Zn}$) metal oxides.

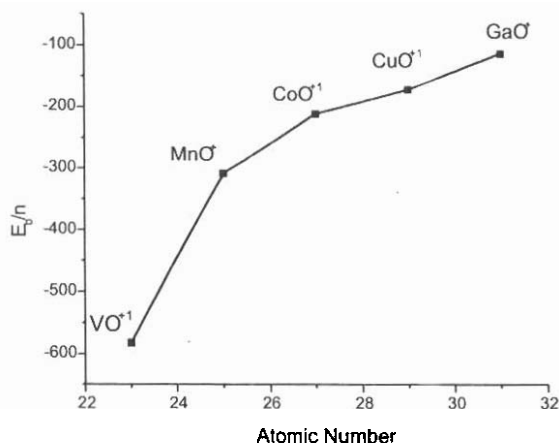


Figure 6. Relationship between the E_b/n ratio at B3LYP/6-31+G(d,p) and the atomic number of the $[MO]^{+1}$ ($M = \text{V, Mn, Co, Cu, Ga}$) metal oxides.

that are greater than the corresponding to ZnO-ethane complex. It is important to note that in these complexes the topology of the C-C bond path behaves as the corresponding for the C=C double bond, indicating the formation of the ethane molecule in the interaction.

These results show that the topologic analysis of the electronic density of the complexes of interaction is able to interpret the nature of the interaction in processes of metal oxide – organic molecules activation.

After the consideration of the interaction metal oxide – ethane for all the studied cases, we can rationalize the corresponding results in terms of both, the d^n configuration of the metal –with some exceptions- and the oxygen bonding energy by electron, which is closely associated to the charge density at the position of the M-O bond of the isolated metal oxides. For the cases of transition metal oxides, the species with low d electrons interacts (high oxygen binding energy by electron) with ethane weakly, giving adsorption complexes only such as Ti and V oxides. Intermediate d configuration, such as d^4 and d^6 interact with ethane giving either alky group of ethanol formation. As are the cases of Cr(II) for the first cases and Mn(III) and Co(III) for the second one. The species have intermediate oxygen binding energy values. Metal oxides with high d configuration interact with ethane with the formation of σ bonds to the hydroxyl and alkyl groups, which are the cases of Ni(II) and Cu(II). For the elements that are not transition metals, such as the Zn and Ga ones, the corresponding oxide compounds have very low oxygen binding energy values that also show the lower charge densities at the M-O bond and at the same time the metals possess the higher formal d configuration (d^{10}). These oxides interact with ethane towards the formation of ethene molecule.

4. Conclusions

The structural and energetic properties of the complexes formed from the chemical activation of ethane (C_2H_6) with a series of neutral ($[MO]^0$, $M = \text{Ti, Cr, Fe, Ni, Zn}$) and charged ($[MO]^+$, $M = \text{V, Mn, Co, Cu, Ga}$) single metal oxides have been investigated by theoretical methods, using the B3LYP hybrid method of the density functional theory DFT in conjunction with the

6-31+G(d,p) basis set. The geometries of these oxides and those of the interaction complexes were fully optimized. The results show that the M—O bonding energies of the charged species are much lower than the corresponding neutral ones. For each series of the studied transition metal oxides, the bonding energies increase with the atomic number of M. The interaction between the C₂H₆ molecule and the metal oxides that was restricted to Cs symmetry leads to the formation of different [C₂H₆-MO] molecular complexes which structural features can be associated, in some cases, to the d electronic configuration of the metal M. The analysis of the topology of the electronic density of the structure of these complexes is able to explain the chemical activation of the C₂H₆ molecule by effect of the metallic oxide, giving important information about the atomic interactions that dominate this activation. These results can be summarized as follows: a) Ti(II)(d²), V(III) (d²) and Fe(II)(d⁶), give [C₂H₆-M] adsorption complexes; b) Cr(II)(d⁴), produce the alkyl and the hydride groups coordinated to the metal by σ bonds (CH₃CH₂-Cr(O)-H); c) Mn(III)(d⁴) and Co(III)(d⁶) activate the ethane towards the formation of ethanol adsorbed on the metal (CH₃CH₂OH-M); d) Ni(II)(d⁸) and Cu(II)(d⁹) activate ethane to the formation of alkyl and the hydroxyl groups coordinated by σ bonds to the metal (CH₃CH₂-M-OH), e) Zn(II)(d¹⁰) and Ga(III)(d¹⁰) give the formation of ethene and water adsorbed to the metal (CH₂CH₂-M-H₂O). The tendencies in the ethane activation can be also rationalized in terms of the oxygen binding energy by electron (E_b/n), property that is closely associated to the charge density at the position of the M-O ionic bond. Finally, the charged oxide species give higher reaction energies than the neutral ones.

Acknowledgment

The present work has been partially supported by the Project of Agenda Petróleo, Fonacit - PDVSA, No. 97003734.

References

1. SHILOV A.E., SHULPIN G.B. *Chem Rev* 97:2879-2932, 1997.
2. AL-ZAHRANI S. M., JIBRIL B.Y., ABA-SAEED A.E. *Ind Eng Chem Res* 39: 4070-4074, 2000.
3. ZEMSKI K.A., JUSTES D.R., CASTLEMAN A.W. Jr. *J Phys Chem A* 105:10237-10245, 2001.
4. SHIOTAY., YOSHIZAWA K. *J Am Chem Soc* 122:12317-12326, 2000.
5. GRACIA L., ANDRÉS J., SAFONT V.S., BELTRÁN A. *Organometallics* 23: 730-739, 2004.
6. PEREIRA M.S., CHAERNASCIMENTO M.A. *Chem Phys Lett* 406: 447-452, 2005.
7. NAKAGAWA K., OKAMURA M., IKENAGA N., SUZUKI T., KOBAYASHI T. *Chem Commun* 9:1025-1026, 1998.
8. DONSI, F., CIMINO, S., PIRONE R., RUSSO, G. *Ind Eng Chem Res* 44: 285-295, 2005.
9. DONSI, F., WILLIAMS, K.A., SCHMIDT, L.D. *Ind Eng Chem Res* 44: 3453-3470, 2005.
10. LIU CH., OZKAN U.S. *J Chem Phys A* 109: 1260-1268, 2005.
11. YODA E., KONDO J.N., DOMEN K. *J Chem Phys B* 109: 1464-1472, 2005.
12. BHASIN M.M. *Topics in Catalysis* Vol. 23, 1-4, 145-149, 2003.
13. PUURUNEN R.L., WECKHUYSEN B.M. *Journal of Catalysis* 210, 418-430, 2002.
14. AIRAKSINEN S.M.K., HARLIN M.E., KRAUSE O.I. *Ind Eng Chem Res* 41, 5610-5026, 2002.
15. Gaussian 98, Revision A.7, FRISCH M.J., TRUCKS G.W., SCHLEGEL H.B., SCUSERIA G.E., ROBBM A., CHEESEMAN J.R., ZAKRZEWSKI V.G., MONTGOMERY J.A., R.E. STRATMANN JR., BURANT J.C., DAPPRICH S., MILLAM J.M., DANIELS A.D., KUDIN K.N., STRAIN M.C., FARKAS O., TOMASI J., BARONE V., COSSI M., CAMMI

- R., MENNUCCI B., POMELLI C., ADAMO C., CLIFFORD S., OCHTERSKI J., PETERSON G.A., AYALA P.Y., CUI Q., MOROKUMA K., MALICK D.K., RABUCK A.D., RAGHAVACHARI K., FORESMAN J.B., CIO-SLOWSKI J., ORTIZ J.V., BABOUL A.G., STEFANOV B.B., LIU G., LIASHENKO A., PISKORZ P., KOMAROMI I., GOMPERTS R., MARTIN R.L., FOX D.J., KEITH T., ALLAHAM M.A., PENG C.Y., NANAYAKKARA A., CHALLACOMBE M., GILL P.M.W., JOHNSON B., CHEN W., WONG M.W., ANDRES J.L., GONZALEZ C., HEADGORDON M., REPLOGLE E.S., POPLER J.A. **Gaussian Inc Pittsburgh PA**, 1998.
16. BECKE A.D. *J Chem Phys* 98: 5648, 1993; LEE C., YANG W., PARR R.G. *Phys. Rev. B*, 37: 785, 1988; MIEHLICH B., SAVIN A., STOLL H., PREUSS H. *Chem Phys Lett* 157: 200, 1989.
17. COLLINS J.B., SCHLEYER P.V.R., BINKLEY J.S., POPLER J.A. *J Chem Phys* 64: 5142, 1967; DOBBS K.D., HEHRE W.J. *J Comput Chem* 8: 880, 1987; GORDON M.S. *Chem Phys Lett* 76: 163, 1980; RAGHAVACHARI K., TRUCKS G.W. *J Chem Phys* 91: 1062, 1989.
18. BADER R.F.W. *Atoms in Molecules: a Quantum Theory*; **Oxford University Press**: Oxford, 1990.
19. Kindly provided by Bader R.F.W. **AIMPAC Program Package**, McMaster University, Hamilton, Ontario (Canada), Versión 94, Rev. B.